Наносистеми, наноматеріали, нанотехнології
Nanosistemi, Nanomateriali, Nanotehnologii
2021, т. 19, № 3, сс. 585–604

PACS numbers: 61.05.cp, 61.72.Hh, 78.20.Ci, 78.30.-j, 78.67.Bf, 81.20.Fw, 81.70.Pg

Structural Characterization of the Metal-Compound Nanosize Tricalcium Phosphate Prepared by Sol–Gel Method

J. Ady[1,2], S. F. Umroati[1], S. Meliana[1], S. D. A. Ariska[1], and D. I. Rudyardjo[1,2]

[1]*Department of Physics,*
Faculty of Science and Technology, Airlangga University,
60115 Surabaya, Indonesia
[2]*Biomedical Engineering Study Program,*
Faculty of Science and Technology, Airlangga University,
60115 Surabaya, Indonesia

The metal compound of nanosize tricalcium phosphate, which is based on lime mineral and phosphoric acid, prepared by the sol–gel method, is investigated. The functional group of tricalcium phosphate is confirmed from the FTIR spectrum results, in which a hydroxyl functional group (–OH) tends to disappear at the temperature of 800°C and 1000°C. With both deficiency optimum number of –OH (3564 cm^{-1}) and increase of the functional groups of PO_4^{3-} (567 cm^{-1} and 601 cm^{-1}) as asymmetry bending and PO_4^{3-} (1039 cm^{-1}, 962 cm^{-1}, and 900 cm^{-1}) as asymmetry stretching vibration modes, the metal compound is formed as tricalcium phosphate (TCP). The crystallographic plane orientations for metastable α-TCP are (001), and for rhombohedral β-TCP, they are (002) and (200), that is found from the XRD results. However, the crystallographic plane orientation for hexagonal α′-TCP is still unformed due to its temperature unreached. Inhomogeneous crystallites of the metal-compound nanosize tricalcium phosphate are confirmed in the relating parameters of crystallite sizes, strains, and dislocations, whereas the crystallinity increases when their temperature increases and is occurred at 800°C and 1000°C with numbers of ≅ 72% and ≅ 77%, respectively. The thermal characterisation is obtained by the specific heat capacity, the fusion and crystallization enthalpies, and weight loss calculated from results of differential scanning calorimetry–thermogravimetric (DSC–TG) and differential thermogravimetric (DTG) analyses.

Досліджено металічну сполуку нанорозмірного трикальційового фосфату, в основі якого є вапняний мінерал і фосфорна кислота, приготовану золь-ґельовим методом. Функціональна група трикальційового фосфату підтверджується результатами Фур'є-спектроскопії інфрачервоних спе-

ктрів, в яких гідроксильна функціональна група (–OH) має тенденцію зникати за температури у 800°C і 1000°C. З обома дефіцитом оптимального числа –OH (3564 $см^{-1}$) і збільшенням функціональних груп PO_4^{3-} (567 $см^{-1}$ і 601 $см^{-1}$) як асиметрії вигинання та PO_4^{3-} (1039 $см^{-1}$, 962 $см^{-1}$ і 900 $см^{-1}$) як асиметрії розтягання в вібраційних модах, металічна сполука утворюється як трикальційовий фосфат (TCP). Кристалографічні орієнтації площин для метастабільного α-TCP є (001), а для ромбоедричного β-TCP вони є (002) і (200), що можна знайти з результатів рентґенівської дифракції. Однак кристалографічна орієнтація площин для гексагонального α′-TCP все ще не сформована через його температуру. Неоднорідні кристаліти металічного нанорозмірного трикальційового фосфату підтверджені у відповідних параметрах кристалітних розмірів, деформацій і дислокацій, тоді як ступінь кристалічности збільшується при підвищенні їхньої температури і відбувається за 800°C і 1000°C з числами ≅ 72% і ≅ 77% відповідно. Термічну характеризацію одержано за рахунок питомої теплоємности, ентальпій синтези та кристалізації, а також втрати ваги, розрахованої за результатами диференціяльної сканувальної калориметрії і термоґравіметричної (DSC–TG) аналізи та диференціяльної термоґравіметричної (DTG) аналізи.

Key words: tricalcium phosphate, sol–gel processing, lime minerals, phosphoric acid.

Ключові слова: трикальційфосфат, золь-ґельове обробляння, мінерали вапна, фосфорна кислота.

(Received 15 October, 2020; in revised form, 19 October, 2020)

1. INTRODUCTION

Tricalcium phosphate is a type of metallic or metal compound that containing a calcium atom (Ca) from alkaline earth metal element and acts as the cation Ca^{2+} in the compound with an anion phosphate PO_4^{3-} in the ionic bonded. Tricalcium phosphate sometimes abbreviated as TCP is a calcium salt of phosphoric acid with a chemical formula $Ca_3(PO_4)_2$. It exists in three groups of the crystalline polymorphs α-, α′-, and β-TCP, which they are used in spinal surgery as bone grafts, bone repair, and remodelling applications [1–3]. The α-TCP designed as a monoclinic structure and it found in the high temperature. However, it can be retained at room temperature as a metastable structure. The stability range of α-TCP strongly depends on the ionic substitutions. The α′-TCP designed as a hexagonal structure is stable as found at the high temperatures too, whilst the β-TCP designed as a rhombohedral structure, which is stable found at below of α- and α′-TCP temperatures [4–6]. They are biocompatible, but more soluble and hydrolyses rapidly to the calci-

um-deficient hydroxyapatite (HA_P) [2]. The β-TCP formations have confirmed at temperature range 500–1100°C by a transformation of the calcium-deficient apatite; it has confirmed in temperature range 710–740°C [7]. The crystalline polymorphs of metal compound tricalcium phosphate have complex structures and refer to numerous materials consisting of calcium ion (Ca^{2+}) together with orthophosphates (PO_4^{3-}) [2, 8–10].

Synthesis of the metal compound tricalcium phosphate most reported by chemical and physical methods: by the chemical method such as precipitation and sol–gel preparations, whilst the physical method such as solid-state preparation. Nowadays, the sol–gel method has been preferred in this work due to simple in the preparation and does not require high temperature in the process, moreover, always results in nanosize particles [2, 11–14]. Subsequently, several studies were reported and have confirmed in Refs. [2, 15–18].

2. EXPERIMENTAL

The sol–gel method preferred in this work, in which the metal compound nanosize tricalcium phosphate resulted. The advantage of the sol–gel method to the sample preparation is a simple treatment and does not require high temperature in the process, moreover, always results in nanosize particles. The process involves the conversion of the monomers into a colloidal solution (sol) that acts as the precursor for an integrated network (gel) of either discrete particles [19–26]. Nowadays, preparation of the metal compound nanosize tricalcium phosphate made from dissolve 1.8 M of $Ca(OH)_2$ with 1.2 M of $H_3(PO)_4$ uses a magnetic stirrer and spin bar for 3 hours at room temperature. Subsequently, the solution stirred again for 8 to 10 hours at 120°C until the wet gel formed. After that, dry form and shrunk gel formations produced through cooled that previous gel form at room temperature for 24 hours. All samples are treated at room temperature, 100°C, 400°C, 800°C, and 1000°C, and have examined by using FTIR [27–30], XRD [31–34], and DSC–TG [35–38]. The FTIR uses for the functional group information of crystalline polymorphs of metal compound nanosize tricalcium phosphate, the XRD uses for the crystallographic confirmation, The DSC–TG, and DTG are used for the thermal characteristic through calculating the specific heat capacity, enthalpy of fusion, and crystallization, and weight loss parameters.

The main materials used in this work, among others there are ethanol (C_2H_6O) with a purity of 96%, calcium hydroxide ($Ca(OH)_2$), and phosphoric acid (H_3PO_4) with the purity of 99% from Pro Analysis material product.

3. RESULTS AND DISCUSSIONS

There are several results from the FTIR spectrum, XRD pattern, DSC–TG, and DTG. FTIR result has confirmed the functional group of metal compound nanosize tricalcium phosphate. Information about the crystallite size, strain, and dislocation, crystallinity and preferential crystallographic plane orientation has found from the XRD results. DSC–TG and DTG results are discussed with the thermal characteristic by calculating the specific heat capacity, enthalpy of fusion and crystallization, and weight loss parameters.

3.1. The FTIR Results and Discussion

Information on the functional group of metal-compound nanosize tricalcium phosphate has been confirmed from the FTIR results. The transmittances number of hydroxyl functional group (–OH) of $Ca(OH)_2$ confirmed is very small or large for the absorbance number, such as shown in Fig. 1, *a*. Subsequently, the transmittances number of –OH decreased or the absorbances number increased for all samples were treated by increased temperature, such as shown in Fig. 1, *b*–*f*. In other words, the deficiency of –OH showed in the formation as a metal compound nanosize tricalcium phosphate while the temperature increased.

Indication of the metastable α-TCP formation looks in the FTIR spectrum at room temperature with –OH functional group deficiency (3446.76 cm^{-1}) and the optimum number of orthophosphates (PO_4^{3-}) appearances as asymmetry bending (567 cm^{-1} and 601 cm^{-1}) and asymmetry stretching vibration mode (1039 cm^{-1}, 962 cm^{-1}, and 900 cm^{-1}) such as shown in Fig. 1, *b*. It is different from the FTIR spectrum of $Ca(OH)_2$, where the functional group of –OH optimum and dominant appeared such as shown in Fig. 1, *a*. Whereas, the $Ca_5(PO_4)_3(OH)$ or hydroxyapatite formation optimum and dominant appeared rather than of β-TCP formation at temperature increased from 100°C to 400°C, such as shown in Fig. 1, *c*–*d*. The β-TCP formation appeared at 800°C and 1000°C optimally and dominantly. Even that, the deficiency of –OH is minimum and almost disappeared. Otherwise, this condition appears PO_4^{3-} (1043.49 cm^{-1}) and PO_4^{-} (605.65 cm^{-1}) functional groups are optimum and dominant such as shown in Fig. 1, *e*–*f*.

3.2. The XRD Results and Discussion

In 1918, P. Scherrer showed that, when parallel monochromatic radiations fall on an oriented random mass of crystals, the diffracted

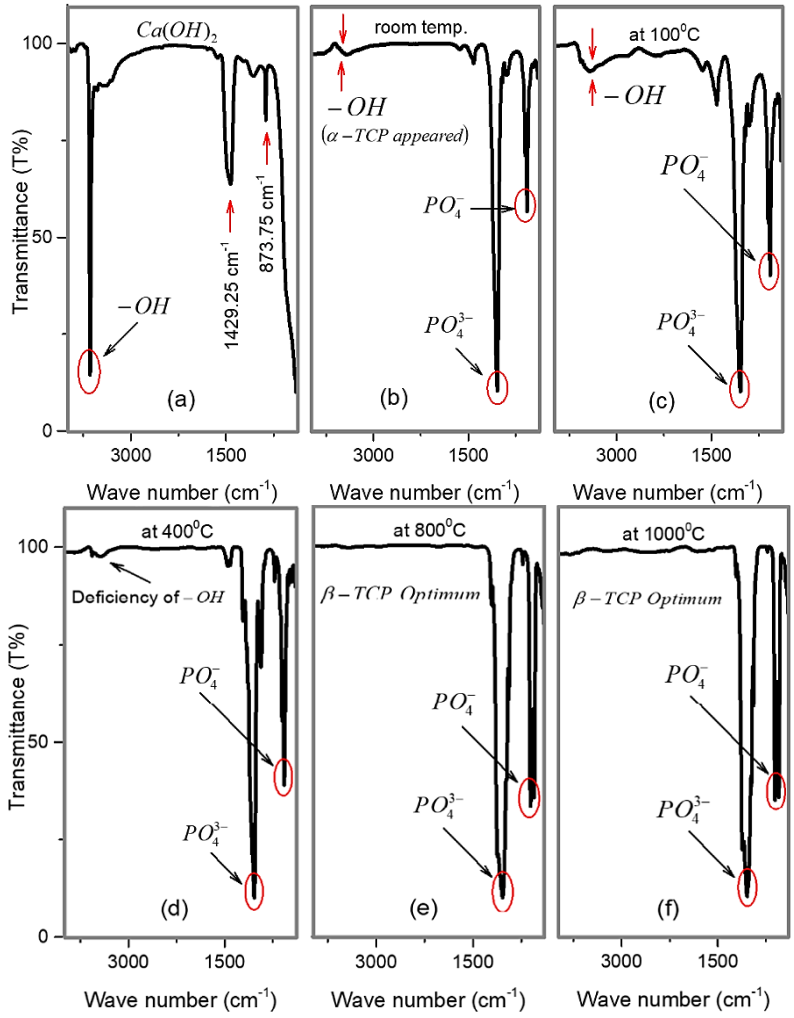

Fig. 1. The FTIR results for calcium hydroxide (*a*) and (*b*)–(*f*) metal compound nanosize tricalcium phosphate samples at various temperatures.

beam is broadened when the particle size is small [39]. The Scherrer equation (also referred to as the Debye–Scherrer equation) applied to estimate the size of zeolite crystallites [40]. The approximation method by Scherrer equation such as in Eq. (1) related to the width of a powder diffraction peak average of the crystallite in polycrystalline powder [40]:

$$D = K\lambda/(\beta_D \cos\theta), \qquad (1)$$

where β_D is the crystallite size contribution to the peak width in ra-

dians, θ is the Bragg angle or a peak position in radians, K is numerical constant near unity, λ is the wave-length of the incident x-rays, and D is the average thickness of the crystal in a normal direction to the diffraction plane hkl or the crystallite size variable from the Scherrer equation. Sample-induced peak broadening is convolution effects caused by the crystallite size and stress. The total sample broadening is usually approximated as a sum of the terms expressed [40–42] in Eq. (2):

$$\beta_T = \beta_D + \beta_\varepsilon , \tag{2}$$

where β_T is the total broadening, β_D is broadening due to crystallite size, and β_ε is the broadening due to strains. From the Scherrer equation, such as Eq. (1), it is found that $\beta_D = K\lambda/(D\cos\Theta)$. Similarly, the XRD-peak broadening due to microstrains is given by $\beta_\varepsilon = 4\varepsilon\tan\theta$. Therefore, the total broadening β_T could be written in Eq. (3) in terms of the reciprocal lattice, the effect of lattice strain is to broaden the reciprocal lattice points to a breadth β_ε, which varies linearly with the distance from the origin [42]:

$$\beta_T = K\lambda/(D\cos\theta) + 4\varepsilon\tan\theta . \tag{3}$$

Multiplication of each side by cosθ yields

$$\beta_T\cos\theta = 4\varepsilon\sin\theta + K\lambda/D . \tag{4}$$

Equation (3) represents a straight line; in it, ε is the gradient or slope of the line, and $K\lambda/D$ is the intercept. Consider the standard equation of the straight line:

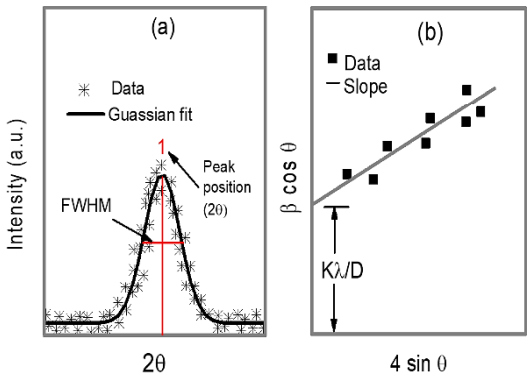

Fig. 2. The Debye–Scherrer equation (DS-method) (*a*) and (*b*) the Williamson–Hall plot method (WH-method).

$$y = mx + c, \tag{5}$$

where m is a slope of the line, and c is the y-intercept. Comparing Eq. (4) with Eq. (5), there are found: $y = \beta_T D\cos\theta$, $m = \varepsilon$, and $c = K\lambda/D$. This method usually named Williamson–Hall plot to the determination of the crystallite size and strain.

The schematic peak position (2θ) and width (FWHM) determinations in the approximation of the Debye–Scherrer method (DS-method) were found by means of the XRD fitted pattern with Gaussian or Lorentzian function used, such as shown in Fig. 2, *a*. Meanwhile, for a given family of the parallel *hkl* planes, it can be plotted βcosθ against 4sinθ. The intercept and slope of the graph from Eq. (4), they are found the crystallite size D and strain ε [40, 42] from Williamson–Hall plot (WH-method), as well as it has shown in the schematic of Fig. 2, *b*. Dislocation density δ is defined as a length of dislocation lines per unit volume of the crystal and calculated by the Williamson–Hall relation, as well as shown in Eq. (6), where dislocation density determination is using the XRD data and based on the broadening of the diffraction lines [43–44]:

$$\delta = D^{-2}, \tag{6}$$

where D is the crystallite size calculated from Eq. (1).

3.2.1. Crystallite Size, Strains, and Dislocations

Figure 3, *a*, *d*, *g*, *j*, *m* show the XRD patterns of metal compound nanosize tricalcium phosphate groups powder after being treated at room temperature, 100°C, 400°C, 800°C, and 1000°C, respectively, whereas Fig. 3, *b–c*, *e–f*, *h–i*, *k–l*, *n–o* show the Gaussian fitted curve with software using for the XRD data. As seen in the Gaussian fit, the peak position for each curve is different, where the fraction of metastable α-TCP appeared at a room temperature and rhombohedral β-TCP appeared at 800°C and 1000°C, respectively, whilst the fraction of α′-TCP still disappeared in this effort due to the temperature has been not reached.

The peak width determination is typically obtained by the fitting curve with Lorentzian, Gaussian, or a combination of the Lorentzian and Gaussian functions. The peak fitting appropriate background correction usually necessary to acquire an accurate assessment of the peak width, especially for peaks, which are partially overlapping. The peak variable is a function of the peak position, peak width, intensity, and mixing parameters [40].

The crystallite size in the D_{DS} and D_{WH} variables have found, and they are different values, such as shown in Fig. 6, *b* and Table 1.

The different yields of the D_{DS} and D_{AHL} values due to influenced by the broadening parameter in the crystallite size determination from the Debye–Scherrer and Williamson–Hall plot methods are different. Debye–Scherrer equation depends on the β_D variable, and Williamson–Hall plot method involves the total broadening β_T such as shown in Eq. (2).

The peak position profiles of the XRD pattern from each sample are shown in Fig. 4, *a*–*i*, while each specific angle and peak has been found the preferential crystallographic plane orientation for metal compound nanosize tricalcium phosphate samples.

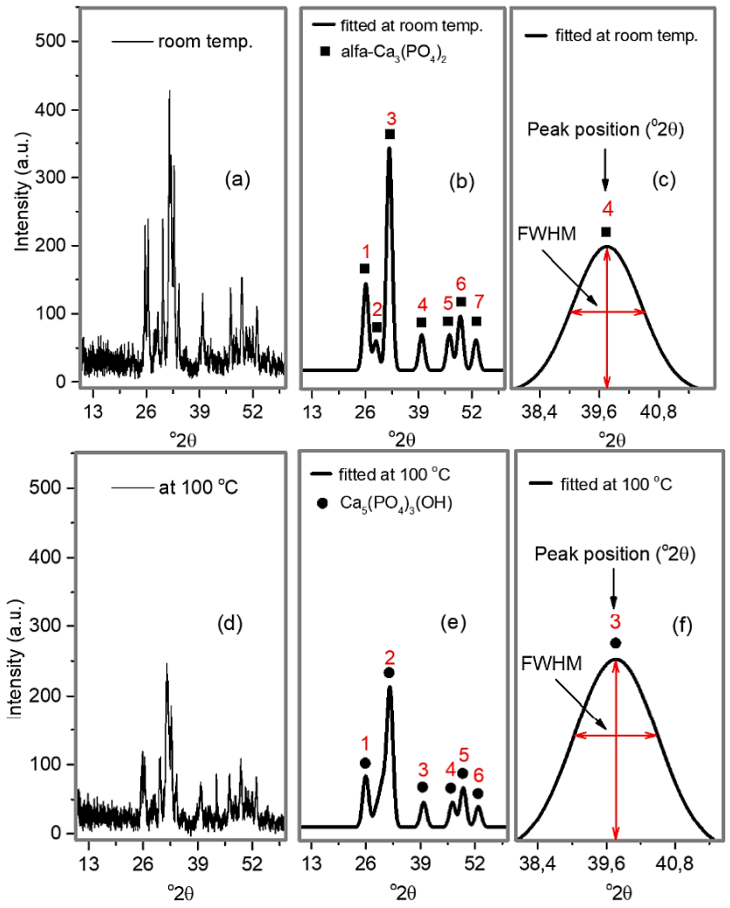

Fig. 3. XRD patterns (*a*), (*d*), (*g*), (*j*), (*m*), the fitting curve (*b*), (*e*), (*h*), (*k*), (*n*), and the peak position (2θ) (*c*), (*f*), (*i*), (*l*), (*o*), and peak width (FWHM) of metal compound nanosize tricalcium phosphate samples in various temperature.

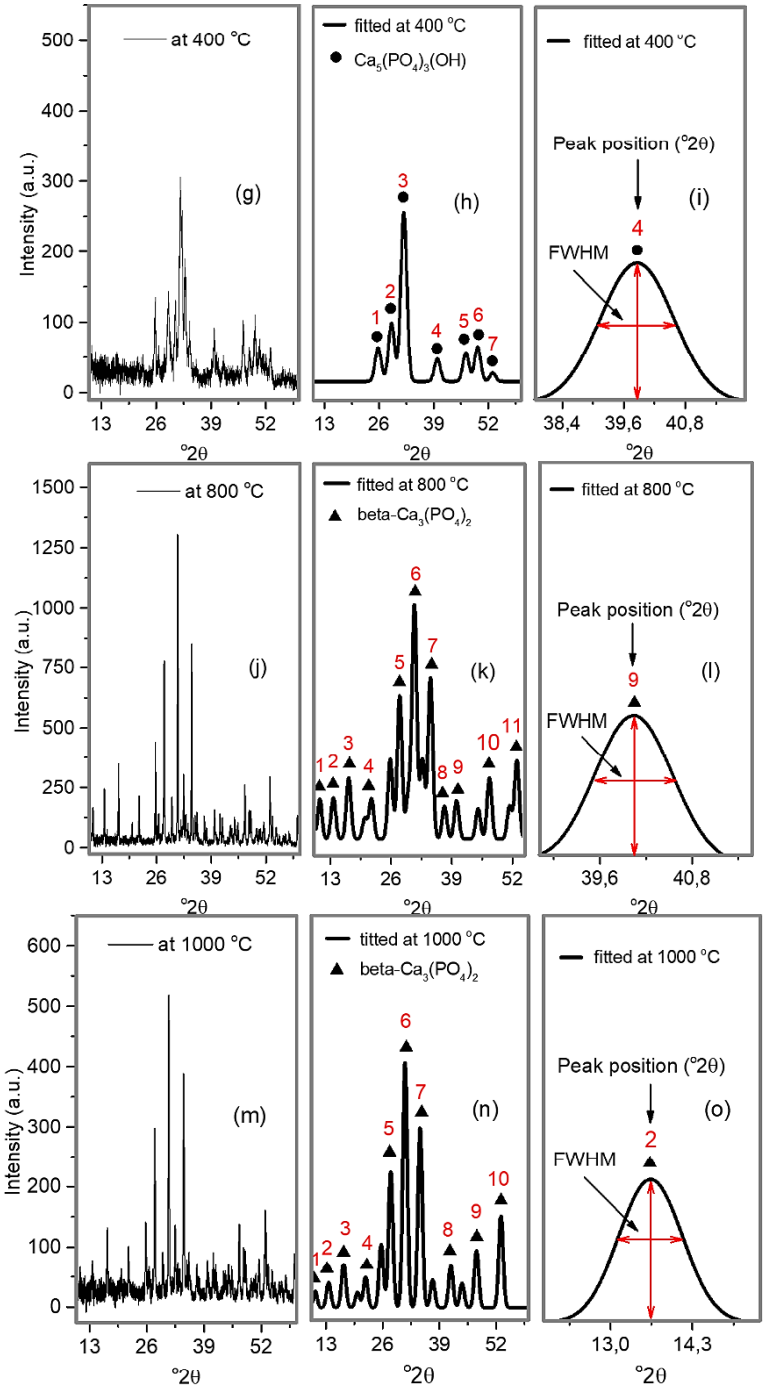

Continuation of **Fig. 3.**

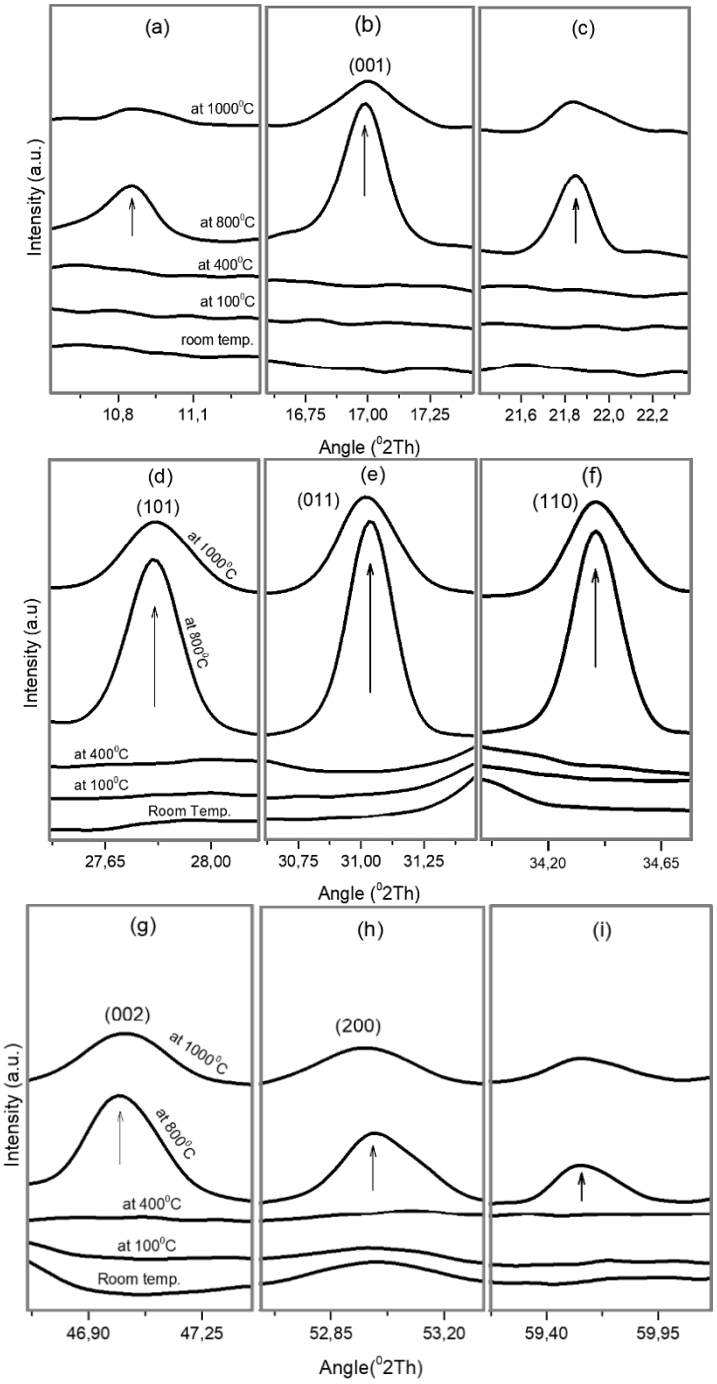

Fig. 4. The peak position for the samples from the XRD pattern *a*–*i* in various specific angles (2θ).

The crystallographic plane (001) is detected at $2\theta \approx 17°$, plane (101)—at $2\theta \approx 27.86°$, plane (011)—at $2\theta \approx 31.06°$, plane (110)—at $2\theta \approx 34.36°$, plane (002)—at $2\theta \approx 47.07°$, and plane (200)—at $2\theta \approx 52.96°$. The optimum peak position appearance at 800°C to 1000°C and minimum peak appearance at room temperature, 100°C, and 400°C. The peak width becomes narrow at 800°C and rather wide at 1000°C, but tends to increase while increase temperature, such as shown in Fig. 4, *a*–*i*.

According to Bragg's law, the moment of the unstrained one crystallite is undergoing diffraction with d, λ, and θ parameters, such as designed in Eq. (7) [45], while the homogenous crystallite is strained or compressed then the d spacing will be changed, where d spacing could be narrow (compressive stress) or wide (tensile stress). If that occurs, say reducing a given spacing (d) to ($d \quad \delta d$), then the peak position (2θ) will be increased to $2(\theta + \delta\theta)$ as well as shown in Eq. (8), whilst, according to Williamson–Hall in Refs. [42], evidence supporting the contention that some of the broadenings are due to particle size is generally less convincing:

$$\lambda = 2d \sin\theta , \tag{7}$$

become

$$\lambda = 2(d - \delta d) \sin(\theta + \delta\theta) . \tag{8}$$

Every crystallite in the sample strained (compressed) by the same amount or its strain in the homogeneous meaning and result in a diffraction peak shifting only, but not broadening. *Vice versa*, that inhomogeneous strains meaning when a different crystallite will be strained in the different amounts and shifted in 2θ due to a structural defect contained. The structural defect factor involves the interstitials, vacancies, dislocations, and layer faults that would induce inhomogeneous strain within a crystallite. The degree of strain obviously being greater at distances close to the actual defect [45]. The approximate relationship relating that mean inhomogeneous strain ε to the peak broadening it produces β_ε. This derived by differentiating Bragg's law and relating the inhomogeneous strain to $\delta d/d$, such as shown in Eq. (2), (3), and (4).

The crystallite strains ε of metal-compound nanosize tricalcium phosphate are found from Eq. (4), such as shown in Fig. 5, *a*–*e* and Table 2, where the crystallite strain is positive for the sample with temperature treatment at 400°C, 800°C, and 1000°C. The values tend to increase, if temperature increases, such as in Fig. 5, *c*–*e*.

This matter could be influenced by the broadening width or peak position parameters increased. However, the crystallite strain for the samples while being treated at room temperature and 100°C are

TABLE 1. Crystallite size of nanosize TCP.

Temperature, °C	D_{DS}, nm	D_{WH}, nm
Room temperature	13.92 ± 0.63	8.02 ± 0.07
100	13.62 ± 0.34	12.27 ± 0,45
400	17.75 ± 0.65	87.75 ± 1.06
800	42.89 ± 0.75	87.21 ± 0.86
1000	67.34 ± 1.05	96.26 ± 1.67

TABLE 2. Crystallite strain and dislocation.

Temperature, °C	$\delta \cdot 10^{-3}$, nm^{-2}	$\varepsilon \cdot 10^{-3}$
Room temperature	15.55	–1,82
100	6.64	–23.4
400	0.13	0.92
800	0.13	1.61
1000	0.11	3.41

negative values. Therefore, the crystallite broadening width β or peak position θ parameters is narrow or declined in the crystal, such as shown in Fig. 5, *a*, *b*, linearly related to the temperature to all crystallite strain yields from Eq. (4) has been shown in Fig. 5, *f*, while its temperature increase, then the crystallite tends to increase too. Subsequently, the crystallite dislocation is found, such as shown in Fig. 6, *a* and Table 2. This matter has shown declined the length of dislocation lines per unit volume in the crystal.

3.2.2. Crystallinity

The crystallinity refers to the structural degree of a solid. There are many materials, such as ceramic-glass, composite, and some polymers being prepared in such a way as to produce a mixture of crystalline and amorphous regions. However, the completely crystalline materials, the perfection of the structural degree could be varied. For example, most alloys are crystalline, but usually comprise many independent crystalline regions (grains or crystallites). In various orientations separated by grain boundaries, where they always contain other crystallographic defects, such as dislocation. That reduces the degree of structural perfection [46].

In this study, the crystallinity of the samples of metal-compound nanosize tricalcium phosphate determined from XRD data by using Eq. (9), where the crystallinity or peak to noise ratio can be calculated by the software using:

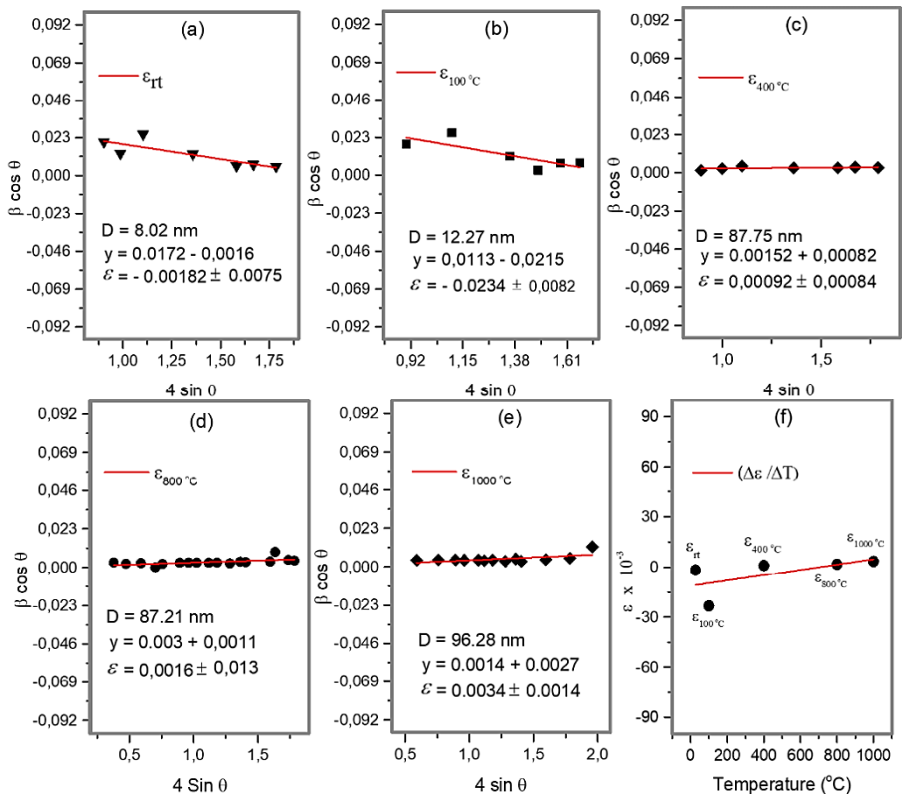

Fig. 5. The crystallite strain (*a*)–(*e*), and (*f*) the relating between the crystallite strain to the temperature of metal compound nanosize tricalcium phosphate sample.

$$K = (A_{CP}/A_{TP}) \cdot 100\%, \tag{9}$$

where K is crystallinity variable in percentage, A_{CP} and A_{TP} are area of the crystalline peaks and all peaks (crystalline + amorphous), respectively. The relating of the crystallinity with temperature has shown in Fig. 6, *c*. This matter indicated that crystallite dislocation in crystal tends to decrease.

3.3. The DSC–TG Results

Differential scanning calorimetry (DSC) and thermogravimetry (TG) are two thermal analysis techniques used in this work, such as shown in Fig. 7, *a*–*c*, where DSC is a technique, in which the heat flow rate difference into a substance and a reference is measured as a function of temperature [36]. TG is a method, in which the mass

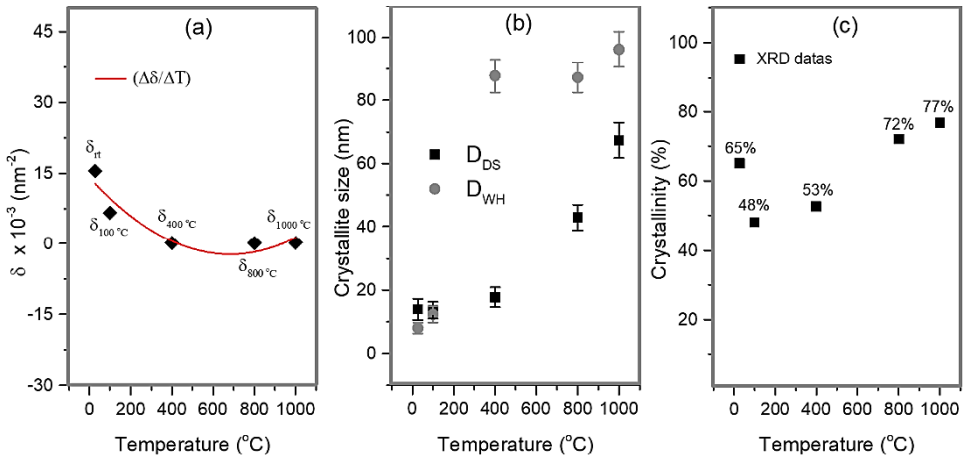

Fig. 6. The crystallite dislocation (*a*), the crystallite size (*b*), and (*c*) the crystallinity of metal-compound nanosize tricalcium phosphate samples at various temperatures.

of a sample is measured over time as the temperature changes. Both measurements are provided with information about the physical properties of the sample, such as phase transition, absorption, adsorption, and desorption [35, 37, 47]. It is a common feature of these techniques that the various characteristic temperature, specific heat capacity, melting and crystallization temperatures, and the heat of fusion as well as the various thermal parameters of the chemical reaction can be determined at constant heating or cooling rate. The major application of the DSC technique is in polymer and pharmaceutical fields, but inorganic and organic chemistry have also benefited significantly from the existence of DSC [36].

3.3.1. Specific Heat Capacity, Enthalpy of Fusion and Crystallization

The DSC result of metal compound nanosize tricalcium phosphate has been confirmed in Fig. 7, *a*–*c*, in which the data about the melting point, specific heat capacity, enthalpy of fusion, and crystallization were obtained. The curve of DSC in Fig. 7, *a*–*c* is shown as a profile curve of the inorganic materials like type in the metal compound.

The fusion and crystallization area in the DSC curve obtained by the plotting of the heat flow to temperature, such as shown in Fig. 8, *a*, the enthalpy of fusion and crystallization were found by compared the heat flow to weigh loss parameters and draw its curve in the relating of $J \cdot s^{-1} \cdot g^{-1}$ versus time, in which the dip peak of curve

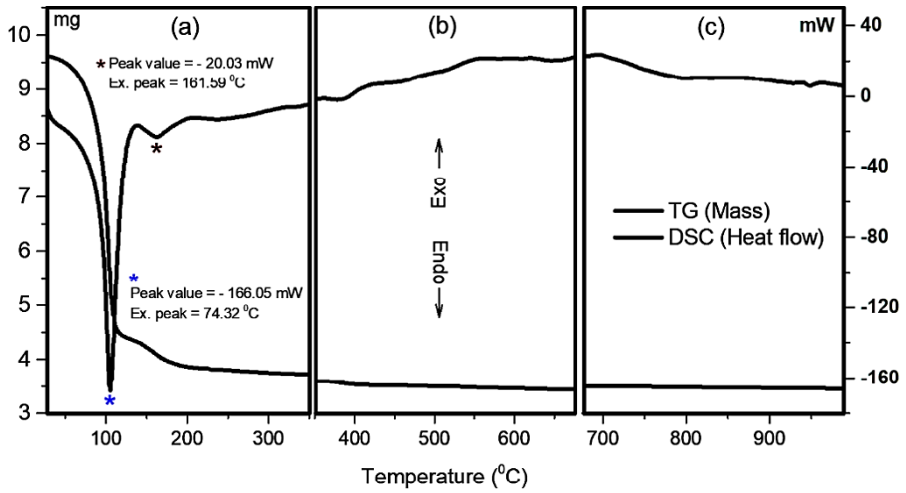

Fig. 7. The profile curves of DSC and TG (*a*)–(*c*) simultaneously for metal-compound nanosize tricalcium phosphate sample at various temperatures.

area Fig. 8, *b* represents the unit enthalpy of fusion and crystallization. The specific heat capacity C_p will be plot temperature on the *x*-axis and for the *y*-axis, and multiply heat flow with time and divide by weight and temperature. The specific number of the melting point, specific heat capacity, enthalpy of fusion, and crystallization were found using appropriate software programming from DSC data, such as shown in Table 3.

Indication of the sample dehydration with large fusion enthalpy of $\Delta H_f \approx 1315.15$ J·g^{-1} occurred by endothermic reaction at range from $T_i \approx 91.23$°C to $T_f \approx 131.08$°C. Subsequently, the crystallization occurred by exothermic reaction with enthalpy $\Delta H_C \approx 40.32$ J·g^{-1}. In this matter, the heat flow is most absorbed to dehydration rather than released to crystallization. The crystallization enthalpy with a large value of $\Delta H_C \approx 133.11$ J·g^{-1} rather than of the enthalpy of fusion $\Delta H_f \approx 7.64$ J·g^{-1} occurred at the range from $T_i \approx 622.94$°C to $T_f \approx 650.91$°C. In this matter, the heat flow most released to crystallization rather than absorbed into dehydration. Therefore, at room temperature, 100°C, 400°C, 800°C, and 1000°C, there are different temperature preferences in this effort based on the DSC result to confirm the effective temperature range for the formation of the metallic-compound nanosize tricalcium phosphate.

3.3.2. The Weight Loss Confirmation

TG is a technique for weight loss or weight increase measurement,

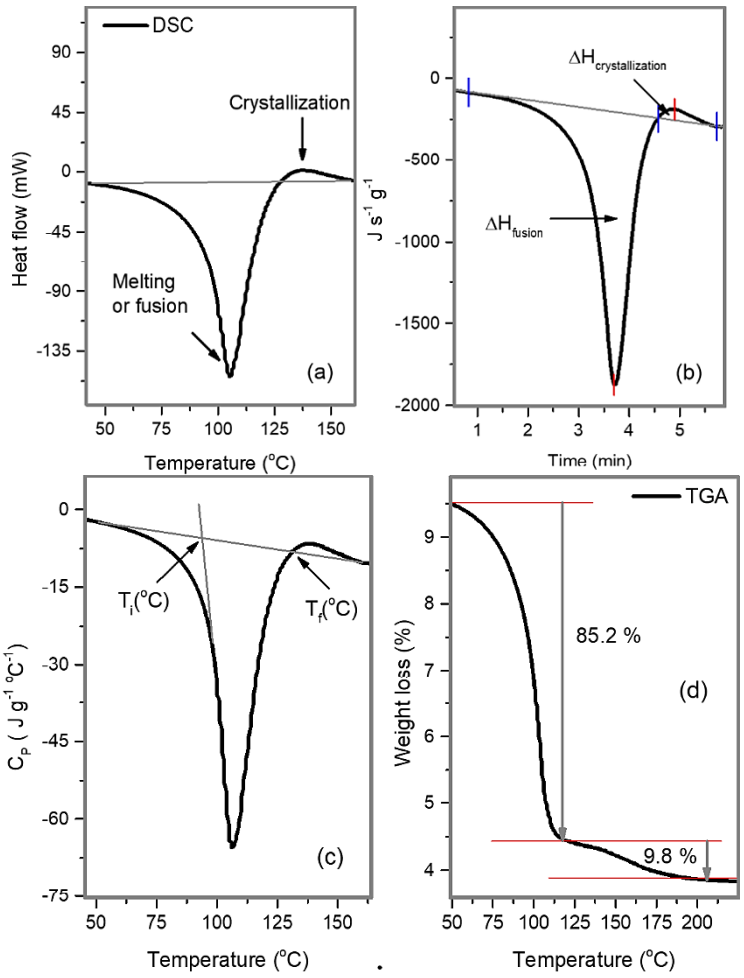

Fig. 8. The fusion and crystallization area (*a*), the fusion and crystallization enthalpies (*b*), the initial and final fusion temperature (*c*), and (*d*) the weight loss of metal compound nanosize tricalcium phosphate sample at various temperatures.

in which the weight of a substance is measured as a temperature function, while a substance is subjected to a controlled temperature program. The TG results of this work are found and shown in Fig. 7.

Separately, the weight loss to temperature curve for specific temperature preferred shown in Fig. 8, *d*, in which the weight loss with a large magnitude of about $\cong 85.2\%$ looks in the range 75–115°C. This matter due to water dehydration occurs in the sample. Subsequently, the volatile substances evaporation occurs in the range 115–185°C. As continued, the intermediate products and

TABLE 3. The fusion and crystallization parameters.

Melting point		Enthalpy of fusion	Enthalpy of crystallization	Specific heat capacity at T_i
T_i, °C	T_f, °C	ΔH_f, J·g^{-1}	ΔH_C, J·g^{-1}	C_P, J·g^{-1}·C^{-1}
91.23	131.08	1315.15	40.32	–5.53
364.45	409.74	59.76	26.37	–0.81
622.94	650.91	7.64	133.11	14.02
941.26	956.82	9.38	10.27	5.15

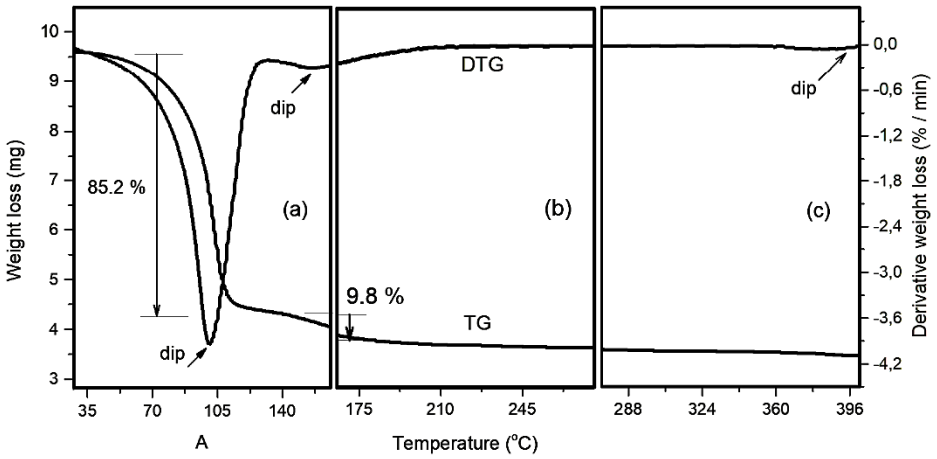

Fig. 9. The profile curves of TG and DTG (*a*)–(*c*) simultaneously of metal-compound nanosize tricalcium phosphate sample at various temperatures.

composition of solid residue, as well as metallic compound residue may form in this temperature range from 27°C to 1000°C. The weight loss of the TG curve probably can hardly be seen so that corresponding temperatures are difficult to determine.

DTG curve is a technique much easier for looking at the temperature corresponding with weight loss or weight increase, in which it is useful to record the first time derivative of the TG curve, due to this, makes the noticing small spot/features on the curve much easier by the dip peaks appear. Therefore, in this work, the dip peak of the DTG curve was identified as much easier seen the weight loss rather than look at the TG curve, such as shown in Fig. 9, *a*–*c* for specific temperature tracking.

4. CONCLUSIONS

The metal-compound nanosize tricalcium phosphate group involves

the metastable α-TCP and rhombohedral β-TCP structures found, in which the crystallite size was in the nanosize scale and inhomogeneous due to the crystallite strain broadening with different values. However, temperature for the hexagonal structure α′-TCP not yet reached in this work.

ACKNOWLEDGMENT

We thank specially to the Faculty of Science and Technology for providing all supports.

REFERENCES

1. B. Liu and D. Xing Lun, *Orthopaedic Surgery*, **4**, Iss. 3: 139 (2012); doi:10.1111/j.1757-7861.2012.00189.x
2. R. G. Carrodeguas and S. De Aza, *Acta Biomaterialia*, **7**, Iss. 10: 3536 (2011); doi:10.1016/j.actbio.2011.06.019
3. A. Reindl, R. Borowsky, S. B. Hein, J. Geis-Gerstorfer, P. Imgrund, and F. Petzoldt, *J. Mater. Sci.*, **49**: 8234 (2014); doi:10.1007/s10853-014-8532-5
4. F. H. Lin, C. J. Liao, K. S. Chen, J. S. Sun, and C. P. Lin, *Biomaterials*, **22**: 2981 (2001); doi:10.1016/S0142-9612(01)00044-8
5. R. Z. Legeros, S. Lin, R. Rohanizadeh, D. Mijares, and J. P. Legeros, *Journal of Materials Science: Materials in Medicine*, **14**: 201 (2003); doi:10.1023/A:1022872421333
6. Y. Li, W. Weng, and K. C. Tam, *Acta Biomaterialia*, **3**: 251 (2007); doi:10.1016/j.actbio.2006.07.003
7. I. R. Gibson, I. Rehman, S. M. Best, and W. Bonfield, *J. Mater. Sci. Mater. Med.*, **12**: 799 (2000); doi:10.1023/A:1008905613182
8. A. Destainville, E. Champion, D. Bernache-Assolant, and E. Laborde, *Mater. Chem. Phys.*, **80**: 269 (2003); doi:10.1016/S0254-0584(02)00466-2
9. E. Champion, *Acta Biomaterialia*, **9**: 5855 (2013); doi:10.1016/j.actbio.2012.11.029
10. S. J. Lee, Y. S. Yoon, M. H. Lee, and N. S. Oh, *Mater. Lett.*, **61**: 1279 (2007); doi:10.1016/j.matlet.2006.07.008
11. K. P. Sanosh, M. C. Chu, A. Balakrishnan, T. N. Kim, and S. J. Cho, *Curr. Appl. Phys.*, **10**: 67 (2010); doi:10.1016/j.cap.2009.04.014
12. C. Zou et al., *Biomaterials*, **26**: 5276 (2005); doi:10.1016/j.biomaterials.2005.01.064
13. J. Duncan et al., *Mater. Sci. Eng. C*, **34**: 123(2014); doi:10.1016/j.msec.2013.08.038
14. J. Pena and M. Vallet-Regí, *J. Eur. Ceram. Soc.*, **23**: 1687 (2003); doi:10.1016/S0955-2219(02)00369-2
15. M. Mathew, L. W. Schroeder, B. Dickens, and W. E. Brown, *Acta Crystallogr. Sect. B: Struct. Crystallogr. Cryst. Chem.*, **B33**: 1325 (1977); doi:10.1107/s0567740877006037
16. M. Yashima and A. Sakai, *Chem. Phys. Lett.*, **372**: 779 (2003); doi:10.1016/S0009-2614(03)00505-0

17. J. C. Elliott, *Structure and Chemistry of the Apatites and Other Calcium Orthophosphates* (Amsterdam: Elsevier: 1994).
18. J. C. Elliot, *General Chemistry of the Calcium*. In: Structure and Chemistry of the Apatites and Other Calcium Orthophosphates (Amsterdam: Elsevier: 2013).
19. G. J. Owens et al., *Progress in Materials Science*, **77**: 1 (2016); doi:10.1016/j.pmatsci.2015.12.001
20. M. Niederberger, *Accounts of Chemical Research*, **40**: 793 (2007); doi:10.1021/ar600035e
21. J. N. Hasnidawani, H. N. Azlina, H. Norita, N.N. Bonnia, S. Ratim, and E. S. Ali, *Proc. Chem.*, **19**: 211 (2016); doi:10.1016/j.proche.2016.03.095
22. R. Vijayalakshmi and V. Rajendran, *Sch. Res. Libr.*, **4**, 2: 1183 (2012); doi:10.11648/j.nano.20140201.11
23. M. M. Pereira, A. E. Clark, and L. L. Hench, *J. Biomed. Mater. Res.*, **6**, 28: 693 (1994); doi:10.1002/jbm.820280606
24. B. H. Fellah and P. Layrolle, *Acta Biomaterialia*, **5**: 735 (2009); doi:10.1016/j.actbio.2008.09.005
25. I. A. Rahman and V. Padavettan, *Journal of Nanomaterials*, **2012**, January, Article ID 132424, 15 pages (2012); doi:10.1155/2012/132424
26. P. Layrolle, A. Ito, and T. Tateishi, *J. Am. Ceram. Soc.*, **81**, No. 6: 1421 (1998); doi:10.1111/j.1151-2916.1998.tb02499.x
27. M. A. Mohamed, J. Jaafar, A. F. Ismail, M. H. D. Othman, and M. A. Rahman, *Fourier Transform Infrared (FTIR) Spectroscopy* (Elsevier Inc.: 2017), p. 3.
28. M. Jackson and H. H. Mantsch, *Crit. Rev. Biochem. Mol. Biol.*, **30**, No. 2: 95 (1995); doi:10.3109/10409239509085140
29. J. Schmitt and H. C. Flemming, *Int. Biodeterior*, **41**: 1 (1998); doi:10.1016/S0964-8305(98)80002-4
30. J. Madejová, *Vibrational Spectroscopy*, **31**: 1 (2003); doi:10.1016/S0924-2031(02)00065-6
31. A. Cassetta, *X-Ray Diffraction (XRD)* (Eds. E. Droli and L. Giorno) (Berlin–Heidelberg: Springer-Verlag: 2014), p. 1.
32. H. Stanjek and W. Hausler, *Hyperfine Interactions*, **154**: 107 (2004); doi:10.1023/B:HYPE.0000032028.60546.38
33. C. G. Kontoyannis and N. V. Vagenas, *Analist.*, **125**: 251 (2000); doi:10.1039/a908609i
34. A. Chauhan, *J. Anal. Bioanal. Tech.*, **5**, No. 5: 212 (2014); doi:10.4172/2155-9872.1000212
35. F. He, W. Yi, and X. Bai, *Energy Conversion and Management*, **47**: 2461 (2006); doi:10.1016/j.enconman.2005.11.011
36. J. D. Menczel and L. Judovits, *Differential Scanning Calorimetry (DSC)* (Eds. R. B. Prime, H. E. Bair, M. Reading, and S. Swier) (New Jersey, Canada: John Wiley and Sons: 2008), p. 1.
37. R. B. Prime, H. E. Bair, S. Vyazovkin, P. K. Gallagher, and A. Riga, *Thermogravimetric Analysis (TGA)* In: Thermal Analysis of Polymers: Fundamentals and Applications (Birmingham: University of Alabama: 2008).
38. V. Rao and J. Johns, *J. Therm. Anal. Cal.*, **92**, 3: 801 (2008); doi:10.1007/s10973-007-8854-5
39. A. L. Patterson, *Phys. Rev.*, **56**: 978 (1939); doi:10.1103/PhysRev.56.978

40. A. W. Burton, K. Ong, T. Rea, and I. Y. Chan, *Microporous Mesoporous Mater.*, **117**: 75 (2009); doi:10.1016/j.micromeso.2008.06.010
41. N. C. Popa, *J. Appl. Cryst.*, **31**: 176 (1998); doi:10.1107/S0021889897009795
42. G. K. Williamson and W. H. Hall, *Acta Metall.*, **1**: 22 (1953); doi:10.1016/0001-6160(53)90006-6
43. Z. Matěj, R. Kužel, and L. Nichtová, *Powder Diffr.*, **25**, No. 2: 125(2010); doi:10.1154/1.3392371
44. T. Ungár and A. Borbély, *Appl. Phys. Lett.*, **69**: 3173 (1996); doi:10.1063/1.117951
45. A. R. Bushroa, R. G. Rahbari, H. H. Masjuki, and M. R. Muhamad, *Vacuum*, **86**: 1107 (2012); doi:10.1016/j.vacuum.2011.10.011
46. M. Chmielová and Z. Weiss, *Appl. Clay Sci.*, **22**, No. 1: 65 (2002); DOI: 10.1016/S0169-1317(02)00114-X
47. D. Giron and C. Goldbronn, *J. Thermal Anal.*, **48**: 473 (1997); doi:10.1007/BF01979494